THE JOURNAL OF BIOLOGICAL CHEMISTRY VOL. 288, NO. 2, pp. 1009–1021, January 11, 2013

Phosphatidylinositol 3-Phosphatase Myotubularin-related Protein 6 (MTMR6) Is Regulated by Small GTPase Rab1B in the Early Secretory and Autophagic Pathways*[S]

Received for publication, June 27, 2012, and in revised form, November 9, 2012 Published, JBC Papers in Press, November 27, 2012, DOI 10.1074/jbc.M112.395087

Yasuhiro Mochizuki[‡1], Riuko Ohashi[§], Takeshi Kawamura[‡], Hiroko Iwanari[‡], Tatsuhiko Kodama[¶], Makoto Naito[§], and Takao Hamakubo[‡]

From the Departments of [‡]Molecular Biology and Medicine and [¶]Systems Biology and Medicine, Research Center for Advanced Science and Technology, The University of Tokyo, Tokyo 153-8904, Japan and [§]Department of Cellular Function, Division of Cellular and Molecular Pathology, Niigata University Graduate School of Medical and Dental Sciences, Niigata 951-8510, Japan

Background: The activity of myotubularin-related protein 6 (MTMR6) is regulated by an unknown mechanism.
Results: The cellular localization of MTMR6 was regulated by Rab1B via the GRAM domain. They were functionally related in the early secretory and autophagic pathways.
Conclusion: MTMR6 is regulated by Rab1B via the conserved GRAM domain.
Significance: Our results reveal a novel regulatory mechanism of MTM phosphatases.

A large family of myotubularin phosphatases dephosphorylates phosphatidylinositol 3-phosphate and phosphatidylinositol 3,5-bisphosphate, which are known to play important roles in vesicular trafficking and autophagy. The family is composed of 16 members, and understanding their regulatory mechanisms is important to understand their functions and related genetic diseases. We prepared anti-myotubularin-related protein 6 (MTMR6) monoclonal antibody and used it to study the regulatory mechanism of MTMR6. Endogenous MTMR6 was present in the cytoplasm and was condensed in the perinuclear region in a microtubule-dependent manner. MTMR6 preferentially interacted with GDP-bound Rab1B via the GRAM domain and partly overlapped with Rab1B in the pericentrosomal and peri-Golgi regions in normal rat kidney cells. Overexpression of GDP-bound Rab1B and the reduction of Rab1B disrupted the localization of MTMR6, suggesting that Rab1B regulates the localization of MTMR6. The reduction of MTMR6 accelerated the transport of vesicular stomatitis virus glycoprotein in which Rab1B is involved. Furthermore, reduction of MTMR6 or Rab1B inhibited the formation of the tubular omegasome that is induced by overexpression of DFCP1 in autophagy. Our results indicate that the cellular localization of MTMR6 is regulated by Rab1B in the early secretory and autophagic pathways. We propose a new regulatory mechanism of myotubularin phosphatase by the small GTPase Rab1B.

MTM1[2] was first identified as the gene responsible for X-linked myotubular myopathy, a severe or fatal muscle weakness in male infants (1). Since then, 15 homologs, called myotubularin-related proteins (MTMRs), have been identified in the human genome (2, 3). MTM1, MTMR1–4, MTMR6–8, and MTMR14 are phosphatidylinositol 3-phosphatasees that dephosphorylate the D-3 position of PI(3)P and PI(3,5)P_2 *in vitro* (3, 4). The other members have been considered to be enzymatically inactive because they lack a conserved cysteine residue that is essential for enzyme activity. However, some of them have been shown to bind to active members and increase the resulting enzyme activity, suggesting that the inactive members are both functional and related to the enzymatic reaction in the cells (5–9). Additionally, MTMR15 was shown to contain DNA repair nuclease activity (10). As a result, although not all of the so-called inactive members have been characterized as yet, they are no longer regarded as merely substrate-trapping proteins.

In addition to *MTM1*, the mutations of several other MTMR genes are involved in various diseases, and certain MTMR knock-out mice display distinct phenotypes. Because MTMR2 forms a heterotetramer with MTMR13 (9), mutation in *MTMR2* and *MTMR13* causes Charcot-Marie-Tooth disease (types 4B1 and 4B2, respectively), a severe autosomal recessive neuropathy in humans (11–13). MTMR5 is another binding protein of MTMR2, and its disruption results in impaired spermatogenesis and azoospermia in mice (14). Mutations of

* This work was supported by the development of New Functional Antibody Technologies of the New Energy and Industrial Technology Development Organization (NEDO), the Funding Program for World-Leading Innovative R&D on Science and Technology (First Program), and Ministry of Education, Culture, Sports, Science and Technology Grant-in-aid for Scientific Research 20221010.

[S] This article contains supplemental Figs. S1 and S2 and Videos 1 and 2.

The nucleotide sequence(s) reported in this paper has been submitted to the DDBJ/GenBank™/EBI Data Bank with accession number(s) AB517623.

[1] To whom correspondence should be addressed: Dept. of Molecular Biology and Medicine, Research Center for Advanced Science and Technology, The University of Tokyo, 4-6-1 Komaba, Meguro-ku, Tokyo 153-8904, Japan. Tel. and Fax: 81-3-5452-5406; E-mail: mochizuki@lsbm.org.

[2] The abbreviations used are: MTM, myotubularin; MTMR, myotubularin-related protein; FYVE, Fab1, YOTB, Vac1, and EEA1; DFCP1, double FYVE domain-containing protein 1; GRAM, glucosyltransferases, Rab-like GTPase activators, and myotubularins; PIKfyve, phosphoinositide kinase, FYVE finger-containing; PI, phosphatidylinositol; PI(3)P, phosphatidylinositol 3-phosphate; PI(5)P, phosphatidylinositol 5-phosphate; PI(3,5)P_2, phosphatidylinositol 3,5-bisphosphate; PI(3,4)P_2, *phosphatidylinositol 3,4-bisphosphate;* NRK, normal rat kidney; VSV-G, vesicular stomatitis virus glycoprotein; UVRAG, UV radiation resistance-associated gene; PX, phox; gp64, glycoprotein 64; COP, *coat protein; endo H,* endo-β-*N*-acetylglucosaminidase H; BFA, brefeldin A; ER, endoplasmic reticulum; pcIC, pericentrosomal domain of the intermediate compartment.

MTMR14 were found in centronuclear myopathy patients (4). MTMR14 knock-out mice exhibit impaired Ca^{2+} homeostasis as well as muscle weakness and fatigue (15). Furthermore, it is reported that single nucleotide polymorphisms (SNPs) in the MTMR9 gene are related to the development of metabolic syndrome (16, 17). These diverse phenotypes strongly suggest that the functions of mammalian MTM phosphatases are not redundant and that they play an essential role in normal cell functions. Interestingly, yeast express only one MTM phosphatase, Ymr1p, and the mutant displays only an elevation of the PI(3)P level (18).

One of the substrates of the MTM phosphatases, PI(3)P, is known to be generated by several different enzyme reactions. Class II PI 3-kinase C2α (PI3K-C2α) and PI3K-C2β are activated by insulin and lysophosphatidic acid, respectively, and generate PI(3)P on the inner leaflet of the plasma membrane (19, 20). Class III PI 3-kinase (VPS34) is involved in the formation of three protein complexes in mammals (21). The VPS34-p150-Beclin1-UVRAG complex is probably the most abundant species among them and generates PI(3)P on the early endosomal membrane. The VPS34-p150-Beclin1-Atg14L complex generates PI(3)P on the omegasome membrane and is involved in the induction of macroautophagy (referred to hereafter as autophagy). The function of the VPS34-p150-Beclin1-UVRAG-Rubicon complex remains elusive (21). PI(3)P is also formed by the dephosphorylation of PI(3,4)P_2 and PI(3,5)P_2 by type Iα inositol polyphosphate 4-phosphatase, 72-kDa 5-phosphatase, or FIG4 lipid phosphatase (22–24). The function of PI(3)P is thought to be the tethering of proteins that contain the FYVE or PX domain to specific membrane compartments (25). PIKfyve binds to PI(3)P via its FYVE domain, phosphorylates the D-5 position of PI(3)P and forms the other substrate of the MTM phosphatases, PI(3,5)P_2 (26). PI(3,5)P_2 is a very low abundance phosphoinositide that is increased by osmotic stress, UV treatment, or interleukin-2 (27, 28). It is related to vesicular trafficking and pH control in the endosomal lysosome system (26). Recent reports revealed that it is also implicated in the degradation step of autophagy in multicellular organisms (29, 30). Considering these substrates are common to all of the MTM phosphatases, the regulatory mechanisms are of considerable interest in terms of understanding the role of each MTM phosphatase and the diverse phenotypes of the aforementioned genetic alterations.

We analyzed MTMR7 to define the function of MTM phosphatases and found that MTMR7 interacts with the ostensibly inactive MTMR9 and further found that recombinant MTMR6 and MTMR9 formed a complex in cells (6). MTMR6 is reported to be involved in the regulation of the Ca^{2+}-activated K^+ channel KCa3.1 (31), apoptosis (32), and autophagy (33) in mammalian cells. Furthermore, *Caenorhabditis elegans* and *Drosophila* MTMR6 is related to the endocytotic machinery (34, 35). These reports suggest that although a mutation in *MTMR6* has not been reported in any human genetic diseases it has a pivotal role in 3-phosphoinositide lipid metabolism in mammalian cells. Nevertheless, although the substrates are known and various biological functions have been proposed for MTMR6, its regulatory mechanism is still poorly understood. In the work presented here, we prepared an anti-MTMR6 monoclonal antibody and clarified the regulatory mechanism of MTMR6.

EXPERIMENTAL PROCEDURES

cDNA Constructs—Mouse MTMR6 and MTMR9 cDNAs were purchased from Invitrogen. Mouse MTMR3 and VSV-G-ts045 (Addgene plasmid 11912 deposited by Dr. Jennifer Lippincott-Schwartz) cDNAs were obtained from Thermo Fisher Scientific and Addgene, respectively. Other cDNAs were amplified by PCR using mouse brain Marathon-Ready cDNA (Clontech) as the template. The cDNA sequences of DFCP1, MTM1, MTMR2, MTMR3, MTMR6, MTMR7, MTMR9, p40phox, Rab1A, Rab1B, and Rab11A corresponded to GenBank™ accession numbers BC050015, NM_001164190, NM_023858, BC081544, NM_144843, NM_001040699, BC145946, FJ168470, NM_008996, NM_029576, and NM_017382, respectively. The full-length MTM phosphatases, MTMR6 Δ-GRAM (amino acids 142–617), MTMR6 Δ-coil (amino acids 1–501), Rab1A, Rab1B, Rab11A, and DFCP1 cDNAs were subcloned into pEF-BOS-Myc, pEF-BOS-HA, pCMV5-Myc, or pEGFP-C1 (Clontech) vectors for expression in mammalian cells. N-terminal EGFP-tagged p40phox-PX domain (amino acids 1–149) was ligated into a pEF4/Myc-His B vector (Invitrogen). N-terminal EGFP-tagged DFCP1, DFCP1 Δ-N (amino acids 417–777), Rab1A, Rab1B, and C-terminal Myc-tagged VSV-G were subcloned into pMXs-Puro retroviral vector (Cell Biolabs, Inc.). To prepare the DFCP1 domain mutant C651S/C770S; DFCP1 S653N/T665A; and Rab1A, Rab1B, and Rab11A mutants, amino acid substitution was performed with a QuikChange site-directed mutagenesis kit (Stratagene). The whole cDNA sequence encoding the baculovirus glycoprotein 64 (gp64) was cut from pBACsurf-1 (Novagen), a transfer plasmid for the baculovirus display system, and ligated into pFastBac1 (Invitrogen) (pFastBac1-gp64). The N terminus of MTMR6 (amino acids 1–100) was subcloned into the multiple cloning sites of pFastBac1-gp64.

Cell Culture and Transfection—COS-7, C2C12, HeLa, NRK, N1E-115, Platinum-E, and RAW 254.7 cells were cultured in DMEM containing 10% FCS. NIH3T3 cells were maintained in DMEM supplemented with 10% calf serum. All media were supplemented with penicillin (100 units/ml) and streptomycin (100 μg/ml), and cells were cultured at 37 °C in a humidified atmosphere of 95% air and 5% CO_2. Mammalian expression constructs were transfected into cells using Lipofectamine 2000™ (Invitrogen) following the manufacturer's protocol, and cells were harvested or used for experiments 48 h after transfection. Stealth™ RNAi synthetic duplexes were purchased from Invitrogen, and the sequences are: rat MTMR6 RNAi: sense, CCAAAUCUCAGAGAUUGACAGUCUU; antisense, AAGACUGUCAAUCUCUGAGAUUUGG; rat Rab1B RNAi: sense, CCGAAUAUGACUACCUGUUUAAGCU; antisense, AGCUUAAACAGGUAGUCAUAUUCGG. A portion of African green monkey MTMR6 cDNA was amplified from COS-7 cell cDNA using mouse PCR primers and sequenced. Based on the cDNA sequence, the following Stealth RNAi synthetic duplexes were designed and transfected into COS-7 cells: GACUACAAGGCUGGCAGCUCAUUGA and UCAAUGAGCUGCCAGCCUUGUAGUC (Invitrogen). The Stealth

RNAi Negative Control kit (Invitrogen) was used as a negative control. All RNAi duplexes were transfected into cells using Lipofectamine RNAiMAX™ (Invitrogen) following the manufacturer's protocol. Retrovirus expression vectors were transfected into Platinum-E packaging cells on a 100-mm dish, and virus-containing medium was collected 72 h after transfection. NRK cells were infected with the retrovirus in the medium supplemented with 8 μg/ml Polybrene and incubated for 3 days. Then the cells were plated on four 150-mm dishes and selected for a week in the medium supplemented with 1 μg/ml puromycin. For starvation, cells were washed three times with PBS, supplemented with 0.9 mM $CaCl_2$ and 0.49 mM $MgCl_2$, and incubated in Earle's balanced salt solution.

Western Blot Analysis—Cells were harvested in a lysis buffer (50 mM Tris-HCl, pH 7.5, 150 mM NaCl, 1 mM EDTA) supplemented with a protease inhibitor mixture (Roche Applied Science) and sonicated briefly. Mouse tissues were homogenized in the same buffer with a Potter-Elvehjem homogenizer and sonicated for 30 s on ice. All cell homogenates were centrifuged at 10,000 $\times$ *g* for 20 min at 4 °C, and the supernatants were collected. The protein concentration of the cell lysates was measured (Bio-Rad) and adjusted to 2.5 μg/μl with SDS sample buffer.

Antibodies—To prepare the anti-MTMR6 monoclonal antibody, the N-terminal MTMR6 and gp64 fusion protein was expressed on the baculovirus membrane, and the whole virus was injected into a gp64 transgenic mouse as the antigen (36, 37). The commercially available antibodies used in this study were monoclonal mouse anti-HA (Sigma); monoclonal mouse anti-Myc, anti-EGFP, polyclonal rabbit anti-Rab1B, and polyclonal goat anti-actin (Santa Cruz Biotechnology, Inc.); polyclonal rabbit anti-β-COP (Calbiochem); monoclonal mouse anti-EEA1 (BD Biosciences); polyclonal rabbit anti-β-tubulin and anti-protein-disulfide isomerase (Cell Signaling Technology Inc.); polyclonal rabbit anti-Atg16L and anti-LC3 (Medical & Biological Laboratories Co., Ltd.); polyclonal rabbit anti-DFCP1 (ProteinExpress Co., Ltd.); and Alexa Fluor 488 goat anti-mouse IgG, Alexa Fluor 594 donkey anti-mouse IgG, and Alexa Fluor 594 goat anti-rabbit IgG (Molecular Probes, Eugene, OR).

Fluorescence Microscopy—Cells cultured on glass coverslips were fixed with 4% paraformaldehyde in PBS for 10 min at room temperature, washed three times with PBS, incubated for 5 min in 0.2% Triton X-100 in PBS, washed three times with PBS, incubated with 2% BSA in PBS for 30 min, and then washed again three times with PBS. Cells were then incubated with primary antibody for 1 h. After three washes with PBS, the cells were incubated for 30 min with fluorescently labeled secondary antibody. The cells were washed three times with PBS and mounted in Gel/Mount™ (Biomeda Corp., Foster City, CA). To visualize recycling endosomes, cells were incubated in FCS-free medium for 1 h at 37 °C. Then the medium was replaced with regular culture medium containing 25 μg/ml Alexa Fluor 594-conjugated human transferrin (Invitrogen) and further incubated for 1 h at 37 °C. Fluorescence images were taken with a microscope (DM LB, Leica) equipped with a cooled charge-coupled device camera (Cool SNAP HQ, Photometrics) and an objective lens (HCX PL APO 63×/1.40–0.60 OIL CS, Leica). The images were acquired using Meta Morph imaging software (v6.2, Molecular Devices).

Immunoprecipitation—The cells were harvested with lysis buffer supplemented with 1% Triton X-100 and a protease inhibitor mixture (Roche Applied Science), sonicated, and centrifuged at 10,000 $\times$ *g* for 20 min at 4 °C. The supernatant was mixed with antibody and rotated for 1 h at 4 °C followed by the addition of protein G-Sepharose beads (GE Healthcare). After rotation for 1 h at 4 °C, the beads were washed three times with the same buffer containing 600 mM NaCl and then mixed with SDS sample buffer.

Size Exclusion Chromatography—COS-7 cells were washed with PBS and harvested with buffer (50 mM Tris-HCl, pH 7.5, 150 mM NaCl, 5 mM EDTA, 10% glycerol) supplemented with a protease inhibitor mixture (Roche Applied Science) and sonicated briefly. Cell homogenates were centrifuged at 10,000 $\times$ *g* for 20 min at 4 °C, and supernatant was collected. An HMW Calibration kit (GE Healthcare) was used as the protein standard, and a 125 μg/ml concentration of each globular protein was mixed with the cell lysate. Samples were applied at a flow rate 0.3 ml/min to a Superdex 200 10/300 GL (GE Healthcare) size exclusion column equilibrated with 50 mM Tris-HCl, pH 7.5, 150 mM NaCl, 5 mM EDTA, 10% glycerol. Fractions (250 μl) were collected, and 3 volumes of ice-cold acetone were added to precipitate the proteins at −20 °C for 2 h. After centrifugation at 17,000 $\times$ *g* for 5 min at 4 °C, the precipitates were dissolved in SDS sample buffer and analyzed by Western blotting.

Proteomics Analysis—Proteomics analysis was carried out as described by Daigo *et al.* (38) with certain slight modifications. Control mouse IgG or anti-MTMR6 antibody was conjugated to Dynabeads protein G (Invitrogen) at a final ratio of 20 mg of antibody/mg of beads. HeLa cells were grown to confluence on two 150-mm dishes and harvested with 10 ml of lysis buffer (50 mM Tris-HCl, pH 7.5, 150 mM NaCl, 1 mM EDTA) supplemented with 1% Triton X-100 and a protease inhibitor mixture (Roche Applied Science). Eluted samples were separated by SDS-PAGE and analyzed by tandem mass spectrometry. For shotgun proteomics, HeLa cells were harvested with lysis buffer supplemented with 0.1% Nonidet P-40 and analyzed as described (38).

Transport Assay—The cells stably expressing VSV-G-Myc were transfected with RNAi duplexes, incubated for 2 days, and further incubated for 12 h at 40 °C. Then the temperature was shifted to 32 °C, and protein synthesis was inhibited by the addition of 100 μg/ml cycloheximide. The cells were harvested with lysis buffer supplemented with 1% Triton X-100 and a protease inhibitor mixture (Roche Applied Science) at each time point and immunoprecipitated with anti-Myc monoclonal antibody. After washing three times with the same buffer, beads were mixed with 0.5% SDS, 40 mM DTT solution and incubated for 10 min at 100 °C. Samples were briefly centrifuged, and an aliquot of supernatant was incubated overnight at 37 °C with or without 625 milliunits/ml endo H (Roche Applied Science) in 50 mM sodium citrate, pH 5.5.

Live Cell Imaging—A stable NRK cell line expressing EGFP-DFCP1 was cultured in Earle's balanced salt solution buffered with 20 mM HEPES, pH 7.5 instead of bicarbonate at 37 °C in ambient atmosphere, and images were captured with a confocal

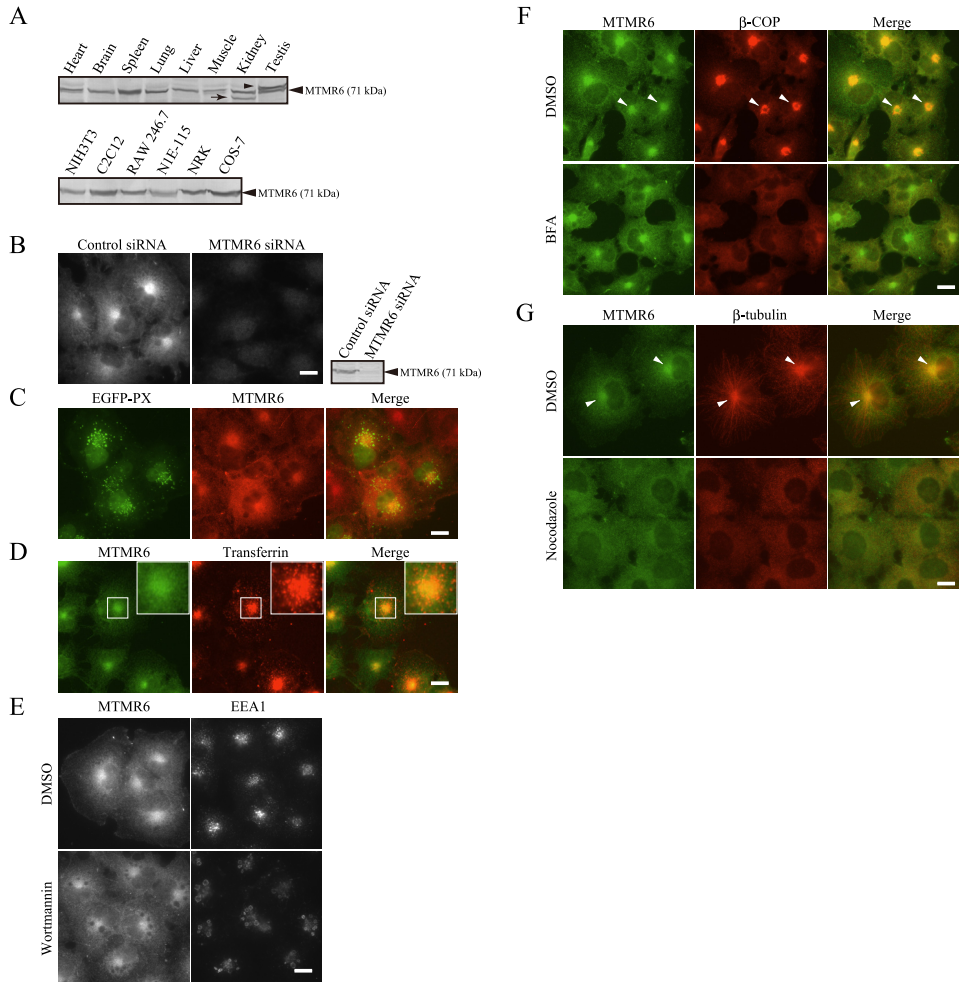

FIGURE 1. **Tissue distribution and cellular localization of MTMR6.** *A*, Western blot analysis of the MTMR6 protein. In the kidney and testis, the extra bands are indicated by the *arrow* and *arrowhead*, respectively. *B*, COS-7 cells stained with an anti-MTMR6 antibody. As a negative control, MTMR6 was knocked down by RNAi. The efficiency of RNAi was confirmed by Western blotting (*right panel*). *C*, COS-7 cells expressing EGFP-PX stained with an anti-MTMR6 antibody. *D*, COS-7 cells were labeled with an Alexa Fluor 594 conjugate of transferrin and the recycling endosome was visualized. MTMR6 was stained with an anti-MTMR6 antibody. The *insets* show the magnified perinuclear region. *E*, COS-7 cells treated with DMSO or wortmannin (100 nM) for 1 h at 37 °C were stained with anti-MTMR6 or anti-EEA1 antibody. *F*, COS-7 cells treated with DMSO or BFA (2 μg/ml) for 1 h at 37 °C were co-stained with anti-MTMR6 and anti-β-COP antibodies. The *arrowheads* indicate the partial overlap of MTMR6 and β-COP. *G*, COS-7 cells were treated with DMSO or nocodazole (100 μM) for 1 h at 37 °C. The cells were co-stained with anti-MTMR6 and anti-β-tubulin antibodies. The *arrowheads* indicate the partial overlap of MTMR6 and a microtubule bundle. In each lane, 100 μg of protein was loaded. *Bars*, 10 μm.

microscope (Fluo View FV1000, Olympus) equipped with an objective lens (PLAPON 60XO, 1.42 numerical aperture, Olympus). For LysoTracker staining, 75 nM LysoTracker Red DND-99 (Invitrogen) was supplemented to the Earle's balanced salt solution.

Electron Microscopy—The cultured cells were fixed with 1.5% glutaraldehyde, postfixed with 1% osmium tetroxide (OsO_4), dehydrated in a graded ethanol series, and embedded in epoxy resin using a Poly/Bed 812 resin kit (Polysciences, Inc., Warrington, PA). Ultrathin sections were observed under electron microscopy (H-800, Hitachi, Tokyo, Japan) after staining with uranyl acetate and lead citrate.

Quantification of the Autophagic and Tube-forming Cells—For each condition, three independent cover glasses were prepared. Under microscopy, fields containing more than five cells were randomly chosen, and 20 such images were captured from each specimen. The cells that contained more than 10 EGFP-DFCP1-positive dots were regarded as autophagic cells. The cells that contained tubes were excluded from the calculation of the autophagic cells.

Real Time PCR—Each cell line was cultured on four dishes, and total RNA was purified with an RNeasy Mini kit (Qiagen). For reverse transcription, 0.5 μg of the total RNA was converted to first strand complementary DNA in 25-μl reactions using TaqMan reverse transcription reagents (Applied Biosystems). Quantitative real time PCR assay was performed with Power SYBR Green PCR Master Mix (Applied Biosystems), and the reaction was run in a CFX96 real time PCR detection system (Bio-Rad). Relative expression levels were calculated using CFX Manager Software version 1.6 (Bio-Rad) using the comparative $\Delta\Delta$Ct method. To detect mouse and rat DFCP1 cDNA simultaneously, DNA sequences that were a perfect match between two animals were chosen and used as PCR primers. The primers used for DFCP1 cDNA were GGCCTGGATGTCCCCTTATC (forward) and GGATTGTATGTCCTCGTTCCC (reverse). Rat glyceraldehyde-3-phosphate dehydrogenase

(GAPDH) was used as a reference gene. The primers for GAPDH cDNA were ATGGTGAAGGTCGGTGTGAA (forward) and GATGGGTTTCCCGTTGATG (reverse).

Image Analysis—Densitometric analyses of Western blotting were performed using the gel analysis macro in ImageJ 1.43u. All fluorescence images were captured at the same instrument settings for quantification and analyzed using ImageJ 1.43u. To determine the amount of MTMR6, the integrated density was measured. Accumulation of MTMR6 was measured by subtracting the threshold density from the integrated density. The appropriate threshold intensity for depicting the peri-Golgi-accumulated MTMR6 was obtained from the images of the control cells.

Statistical Analysis—Statistical significance was determined using a two-tailed unpaired *t* test as performed in Excel software unless otherwise indicated. Comparisons of multiple groups were performed using a two-way analysis of variance followed by post hoc testing using the Holm-Sidak method in SigmaPlot software (Systat Software, Inc.).

RESULTS

Tissue Distribution and Cellular Localization of MTMR6—We prepared anti-mouse MTMR6 monoclonal antibodies using a baculovirus expressing an N-terminal MTMR6 and gp64 fusion protein as the antigen (36, 37). We first analyzed the tissue and cellular distribution of MTMR6 by Western blotting. A monoclonal antibody (clone Y67002) detected a 71-kDa band by Western blotting, and MTMR6 was expressed in all of the mouse tissues and cell lines examined (Fig. 1*A* and supplemental Fig. S1A). The extra band in the testis was thought to be a splicing isoform of MTMR6 because we found mRNA containing an insertion from mouse testis (GenBank accession number AB517623) (supplemental Fig. S1B). The kidney extra band has not yet been identified.

To gain insight into the regulatory mechanism of MTMR6, the intracellular localization was analyzed by immunofluorescence. When COS-7 cells were stained with an anti-MTMR6 antibody, a strong signal was observed in the perinuclear region, and the cytosol was also faintly stained (Fig. 1*B*). MTMR6 RNAi resulted in the disappearance of these signals, confirming that the signals showed the actual localization of the endogenous MTMR6 in cells (Fig. 1*B*). As shown in Fig. 1*C*, the dense perinuclear MTMR6 was partially overlapped with PI(3)P-positive granules that were visualized with EGFP-PX. It was also partly overlapped with the recycling endosome marker transferrin in the perinuclear region (Fig. 1*D*). However, the staining pattern of MTMR6 was not granular, and MTMR6 was not observed at these transport vesicles (Fig. 1, *C* and *D*, *inset*). The GRAM domain is conserved between mammalian MTM phosphatases and has been shown to bind to several 3-phosphoinositide lipids on the membrane (39–41). When COS-7 cells were treated with a relatively high dose of the PI 3-kinase inhibitor wortmannin (100 nM), perinuclear localization of MTMR6 was not disrupted, although the PI(3)P-rich EEA1-positive granules were aberrantly vacuolated (Fig. 1*E*). The cluster of MTMR6 was partially overlapped with the Golgi marker β-COP but was resistant to the Golgi-disrupting reagent brefeldin A (BFA) (Fig. 1*F*). The cluster of MTMR6 was also closely overlapped with the microtubule bundle at the perinuclear region (Fig. 1*G*). When COS-7 cells were treated with the microtubule-disrupting reagent nocodazole, the MTMR6 cluster completely disappeared, coincident with the disruption of the microtubule network (Fig. 1*G*). These data show that MTMR6 is a ubiquitously expressed cytosolic enzyme, which condenses in the pericentrosomal region in a microtubule-dependent manner.

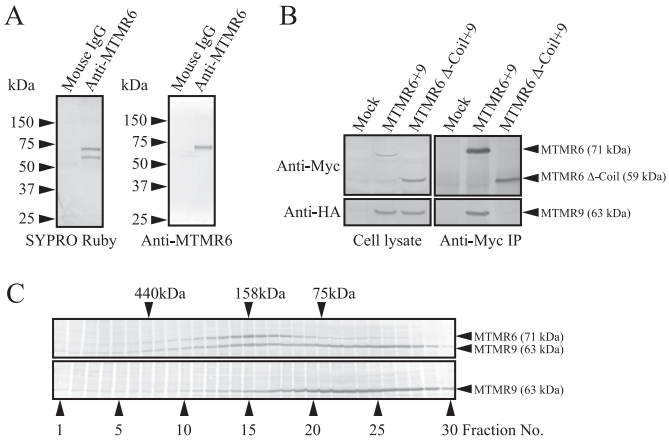

FIGURE 2. **Characterization of the MTMR6 enzyme complex.** *A*, isolation of the MTMR6 enzyme complex. Endogenous MTMR6 was immunoprecipitated from HeLa cell lysate with an anti-MTMR6 antibody. *Left*, SYPRO Ruby staining. *Right*, Western blotting with the anti-MTMR6 antibody. The *numbers* depicted on the *left* are molecular mass markers. *B*, identification of the MTMR9-binding domain of MTMR6. Myc-tagged MTMR6 and MTMR6 Δ-coil were co-expressed with HA-tagged MTMR9 in COS-7 cells. Myc-tagged proteins were immunoprecipitated with an anti-Myc antibody. *C*, size exclusion chromatography of MTMR6-MTMR9 complex. COS-7 cell lysates that expressed HA-tagged proteins were separated by a size exclusion column. Each fraction was analyzed by Western blotting with an anti-HA antibody. The molecular weight standards shown in the figure are ferritin (M_r = 440,000), aldolase (M_r = 158,000), and conalbumin (M_r = 75,000). *IP*, immunoprecipitation.

Characterization of the MTMR6 Enzyme Complex—The cellular localization of MTMR6 prompted the speculation that MTMR6 forms a protein complex and that its binding protein accumulates the enzyme in that region. Hence, endogenous MTMR6 was immunoprecipitated from HeLa cell lysate and analyzed by SDS-PAGE. When the gel-separated proteins were stained with SYPRO Ruby, two anti-MTMR6 antibody-specific bands were clearly evident in the gel (Fig. 2*A*, *left panel*). These bands were identified as MTMR6 and MTMR9 by Western blotting and liquid chromatography-tandem MS (LC/MS/MS) (Fig. 2*A*, *right panel*, and supplemental Fig. S2, A and B). These results show that endogenous MTMR6 interacts with MTMR9 and that MTMR9 is the major binding protein of MTMR6. Deletion of the coiled coil domain abolished the association of Myc-MTMR6 and HA-MTMR9, indicating that they interact via the coiled coil domain (Fig. 2*B*). To estimate the size of the complex, the cell lysate expressing HA-MTMR6 and HA-MTMR9 was separated by size exclusion chromatography. As shown in Fig. 2*C*, *upper panel*, their complex was soluble and mainly found in fraction 15, which contained the 158-kDa marker aldolase. When the cell lysate containing only HA-MTMR9 was separated, the main peak was found near the 75-kDa marker (Fig. 2*C*, *lower panel*), confirming that the proteins found in fraction 15 are the complex. The deduced molec-

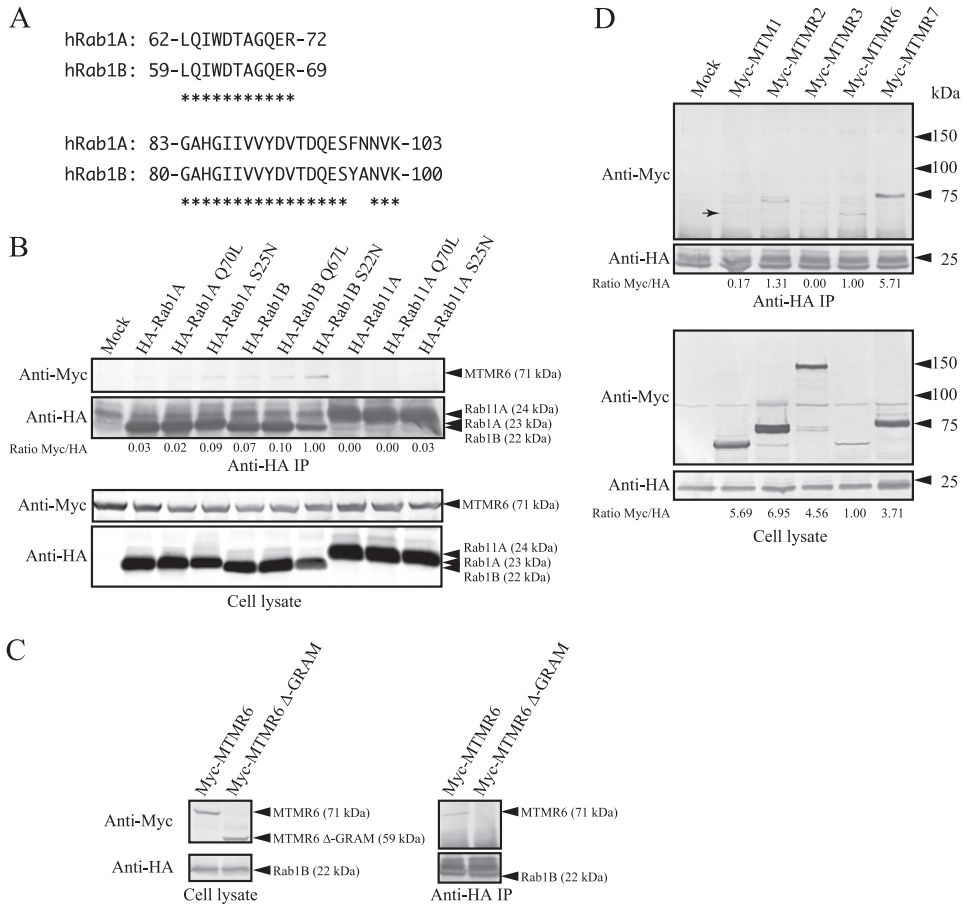

FIGURE 3. **Identification of the low affinity binding protein for MTMR6.** *A*, the amino acid sequence of tryptic peptides of human Rab1B identified by shotgun proteomics. For comparison, the corresponding region of human Rab1A is aligned. *Asterisks* indicate amino acids homologous between hRab1A and hRab1B. *B*, interaction of MTMR6 and several Rab proteins. Myc-tagged MTMR6 was co-expressed with HA-tagged Rab proteins in COS-7 cells and immunoprecipitated with an anti-HA antibody. Densitometric Myc/HA ratios of immunoprecipitate are shown under the blot. *C*, identification of the Rab1B-binding domain of MTMR6. Myc-tagged MTMR6 and MTMR6 Δ-GRAM were co-expressed with HA-tagged Rab1B S22N in COS-7 cells. The HA-tagged protein was immunoprecipitated with the anti-HA antibody. *D*, interaction of several MTM phosphatases and Rab1B S22N. Myc-tagged MTM phosphatases were co-expressed with HA-tagged Rab1B S22N in COS-7 cells and immunoprecipitated with the anti-HA antibody. The *arrow* indicates MTM1. The *numbers* depicted on the *right* are molecular mass markers. Densitometric Myc/HA ratios of immunoprecipitate and cell lysate are shown under the blot. *IP*, immunoprecipitation.

ular mass of the MTMR6-MTMR9 heterodimer is 134-kDa, and their complex is estimated to be a heterodimer. Hence, the soluble MTMR6-MTMR9 complex is a heterodimer and does not contain the stable binding protein that determines the cellular localization of the complex.

Identification of the Low Affinity Binding Protein for MTMR6—Searching for low affinity binding proteins for MTMR6, we further used a shotgun proteomics approach to analyze all of the proteins immunoprecipitated with the anti-MTMR6 antibody. As a result, several Golgi-related proteins were identified in the immunoprecipitate. A small GTPase, Rab1B, was one of the candidates for the MTMR6-interacting protein, and the amino acid fragments detected in the immunoprecipitate are shown in Fig. 3*A*. The amino acid sequence of Rab1B is similar to that of Rab1A, but the Rab1A-specific fragment was not detected by LC/MS/MS analysis. Because Rab1A and Rab1B are similar proteins and Rab11A localizes in the pericentrosomal region (42), the binding of these proteins and their GTP- (Rab1A Q70L, Rab1B Q67L, and Rab11A Q70L) and GDP-restricted mutants (Rab1A S25N, Rab1B S22N, and Rab11A S25N) to MTMR6 was examined. MTMR6 associated with Rab1A and Rab1B and preferentially bound to the Rab1B S22N mutant (Fig. 3*B*). MTMR6 was scarcely bound to Rab11A or its mutants (Fig. 3*B*). These results were reproducible, and therefore, Rab1B is a prime candidate for a low affinity binding protein for MTMR6. Deletion of the GRAM domain abolished the binding of Rab1B S22N and MTMR6, indicating that Rab1B binds to MTMR6 via the GRAM domain (Fig. 3*C*). Because the GRAM domain is conserved in mammalian MTM phosphatases, the binding of Rab1B S22N and other MTM phosphatases was further analyzed by immunoprecipitation. As shown in Fig. 3*D*, the signals of MTM phosphatases, except for MTMR3, were detected in the immunoprecipitate. Comparison of the ratios of the Myc-tagged proteins in the immunoprecipitate and cell lysate suggests that the phylogenetically close MTMR6 and MTMR7 are preferentially bound by Rab1B S22N.

These results suggest that Rab1B is either weakly or transiently associated with MTMR6 via the GRAM domain and that its interaction to MTMR6 is regulated by GDP/GTP nucleotide exchange. In addition to MTMR6, MTMR7 may be associated with Rab1B in cells.

Cellular Localization of MTMR6 and Rab1B—Because the interaction of MTMR6 and Rab1B protein had been confirmed by immunoprecipitation, the cellular localization of MTMR6

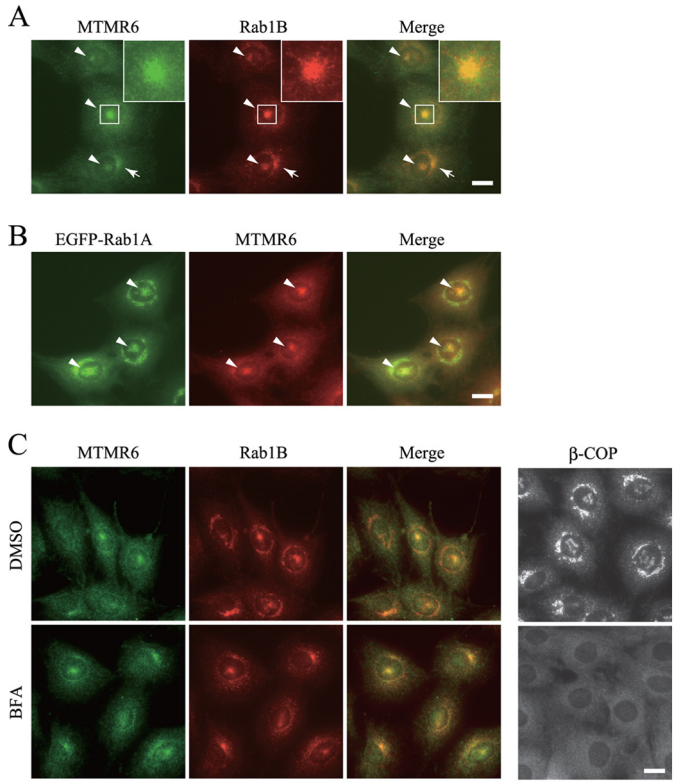

FIGURE 4. **Cellular localization of MTMR6 and Rab1B in NRK cells.** *A*, immunostaining of NRK cells with anti-MTMR6 and anti-Rab1B antibodies. The *arrowheads* indicate MTMR6 and Rab1B concentrated at the cell center. The *arrows* indicate the peri-Golgi-localized MTMR6 and Rab1B. The *insets* show an enlarged view of the magnified *boxed* regions. It should be noted that the size and shape of the MTMR6 and Rab1B stainings are correlated in these three cells even if they are not completely overlapped. *B*, stable NRK cell line expressing EGFP-Rab1A was stained with anti-MTMR6 antibody. The *arrowheads* indicate EGFP-Rab1A and MTMR6 concentrated in the pericentrosomal region. *C*, NRK cells treated with DMSO or BFA (2 μg/ml) for 1 h at 37 °C were stained with anti-MTMR6 and anti-Rab1B antibodies or anti-β-COP antibody, respectively. *Bars*, 10 μm.

and Rab1B was further analyzed. When NRK cells were stained with the anti-MTMR6 antibody, a dense cluster of MTMR6 was observed at the cell center (Fig. 4*A*). The cells were also stained in the peri-Golgi region and the cytosol (Fig. 4*A*). Rab1B was observed at the cell center, at the peri-Golgi region, and as peripheral dots (Fig. 4*A*). At the cell center and the peri-Golgi region, the MTMR6 and Rab1B staining patterns were partially overlapped, and their size and shape were correlated (Fig. 4*A*). Marie *et al.* (43) reported that Rab1A is observed at the Golgi apparatus and close to the ER exit site, and a Rab1A-containing membrane cluster is frequently separated from the Golgi apparatus in NRK cells. Such a membrane cluster is located around the microtubule-organizing center and sometimes observed below the nucleus. They showed that the cluster mediates ER-Golgi trafficking and termed it the "pericentrosomal domain of the intermediate compartment" (pcIC). The staining pattern of MTMR6 and Rab1B was very similar to that of Rab1A, and the dense cluster of MTMR6 is reminiscent of the pcIC. When a stable NRK cell line expressing EGFP-Rab1A was stained with an anti-MTMR6 antibody, the signals were partially overlapped at the cell center, confirming that MTMR6 is highly concentrated in the pcIC region along with Rab1B (Fig. 4, *A* and *B*). To further characterize the localization of MTMR6 and Rab1B in the pcIC, NRK cells were treated with BFA, and the effect on each protein was compared. As shown in Fig. 4*C*, MTMR6 was resistant to BFA in the pcIC and the peri-Golgi regions. Rab1B was diffuse but retained by BFA treatment in both regions in sharp contrast to β-COP (Fig. 4*C*). Therefore, their localization is resistant to BFA in these compartments, and this is consistent with Rab1A (43). These results show that the localization patterns of MTMR6 and Rab1B are closely related in the pcIC, the way station of ER-Golgi membrane trafficking.

Effect of Rab1B Mutants on the Localization of MTMR6—As shown in Fig. 3*B*, the affinity of Rab1B to MTMR6 was different depending on the GDP and GTP state of Rab1B. Therefore, Rab1B, Rab1B Q67L, or Rab1B S22N was overexpressed in NRK cells, and their effect on the localization of MTMR6 was further examined. Rab1B and Rab1B Q67L were localized at the pcIC and the peri-Golgi regions, and Rab1B Q67L increased peri-Golgi vacuoles in NRK cells (Fig. 5*A*). Their expression did not show an apparent effect on the localization of MTMR6. By contrast, Rab1B S22N was observed in the cytosol as reported (44), and the accumulation of MTMR6 was abolished in the cells expressing Rab1B S22N (Fig. 5*A*). These data suggest that GDP-bound Rab1B interacts with MTMR6 in cells and can change the localization of MTMR6.

To confirm the results of our microscopic observation, stable cell lines expressing EGFP-tagged Rab1B or its mutants were prepared, and their effect on the accumulation of MTMR6 was quantitatively analyzed using image analysis. As shown in Fig. 5*B*, the accumulation of MTMR6 was unequivocally reduced in EGFP-Rab1B S22N-expressing cells in accordance with the results of microscopic observation. Quantitative analysis further revealed that EGFP-Rab1B Q67L also significantly reduced MTMR6 accumulation. The total amount of MTMR6 was slightly reduced in the cells expressing Rab1B mutants. A slight reduction in MTMR6 was also detected by Western blotting in cells expressing EGFP-Rab1B S25N (Fig. 5*C*). However, the extent of reduction was very small compared with the reduction in accumulation (Fig. 5*B*). Consequently, our results indicate that Rab1B mutants disrupt the accumulation of MTMR6. In our stable cell lines, expression levels of EGFP-Rab1B and Rab1B Q67L were comparable with that of endogenous Rab1B, but that of EGFP-Rab1B S22N was quite low (Fig. 5*C*). These data suggest that the balance of GDP- and GTP-bound Rab1B protein is important for the efficient accumulation of MTMR6 and that GDP-bound Rab1B plays a major role in the localization of MTMR6.

Interaction of MTMR6 and Rab1B in the Early Secretory Pathway—To gain further insight into the interaction of MTMR6 and Rab1B, the expression of endogenous proteins was reduced by RNAi, and the effects were analyzed. When Rab1B was knocked down, the cluster of MTMR6 was diffused in the pcIC region, and the peri-Golgi MTMR6 was also dispersed into the cytosol (Fig. 6*A*). This observation was confirmed by quantitative image analysis (Fig. 6*B*). The expression of MTMR6 was slightly reduced by Rab1B RNAi, but its influence on our results was considered to be small (Fig. 6*D*). These results show that Rab1B regulates the localization of MTMR6 in the pcIC and the peri-Golgi regions.

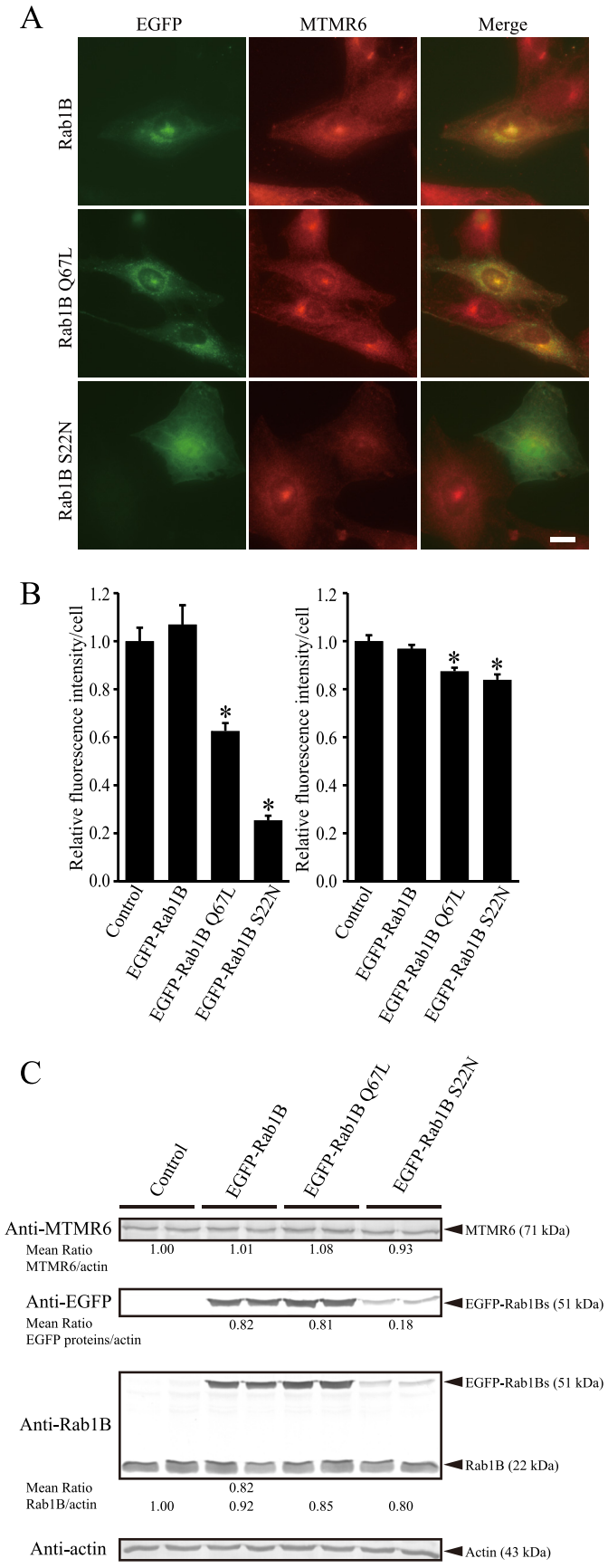

FIGURE 5. **The effect of the GDP- and GTP-restricted forms of Rab1B on the localization of MTMR6.** *A*, NRK cells were transiently transfected with EGFP-tagged Rab1B, Rab1B Q67L, or Rab1B S22N and stained with an anti-MTMR6 antibody. *B*, *left*, amount of MTMR6 accumulated in the cell. *Right*, total amount of MTMR6 in the cell. The stable cell lines were stained with anti-MTMR6 antibody, and the relative fluorescence intensity of each cell was determined by image analysis. Non-infected NRK cells were used as a control. Each cell line was cultured on four cover glasses, and 10 images were acquired from each specimen. The average fluorescence intensity/cell was determined for each image, and the data from 40 images were analyzed for each cell line. The bar graph shows the average of three independent experiments. The values were normalized to the mean intensity of the control. All *asterisks* indicate a significant difference from the control (mean ± S.E. (*error bars*); $n = 120$; *, $p < 0.001$). *C*, the expression levels of MTMR6, Rab1B, and EGFP-tagged Rab1B proteins were compared between the stable cell lines expressing EGFP-tagged Rab1B and its mutants by Western blotting. Quantification was performed in duplicate, and 100 μg of protein was loaded in each lane. The bands were quantified by densitometry, and actin was used as a loading control. Because the affinity of anti-Rab1B antibody to EGFP-Rab1B S25N was lower than that to other Rab1B proteins, the amount of EGFP-tagged proteins detected with anti-EGFP antibody was normalized to that of EGFP-Rab1B detected with anti-Rab1B antibody. Non-infected NRK cells were used as a control. *Bar*, 10 μm.

Rab1B regulates ER-Golgi and intra-Golgi trafficking (45). We therefore knocked down levels of MTMR6 in NRK cells and examined the effect on the ER-Golgi transport of VSV-G. There was no effect on the accumulation of VSV-G in the ER by MTMR6 RNAi (Fig. 6*C*, 0 min). At the 15-min time point, the ratio of the endo H-resistant VSV-G protein was significantly higher in MTMR6 siRNA-treated cells than in control cells. At the 30-min time point, the difference became small, but the ratio was still significantly higher in MTMR6 siRNA-treated cells, indicating that the transport of VSV-G from the ER to the Golgi was accelerated by MTMR6 siRNA. The expression level of Rab1B was not altered by MTMR6 RNAi (Fig. 6*D*). These results indicate that MTMR6 is involved in the secretory pathway with Rab1B and negatively regulates ER-Golgi protein transport.

Involvement of MTMR6 and Rab1B in Regulation of the Omegasome—Rab1B is observed in the autophagosome, and MTMR6 and Rab1B have been suggested to be involved in autophagy (33, 46, 47). Therefore, to further define the functional relationship between MTMR6 and Rab1B, their relation to autophagy was examined. The omegasome is a donut-shaped ring structure that is generated on the ER in the autophagic condition and enriched with PI(3)P (48). Some sort of autophagosome is generated from omegasomes. EGFP-DFCP1 is able to detect PI(3)P on the omegasome and has been utilized as an autophagosome marker in recent reports (47–50). Therefore, a stable NRK cell line expressing EGFP-DFCP1 was used to monitor autophagy.

First, the cells were treated with control, MTMR6, or Rab1B RNAi, and the number of autophagic cells was counted under normal and starved conditions. The number of autophagic cells was not affected by MTMR6 or Rab1B RNAi in this experiment (Fig. 7*A*). Instead, we found that DFCP1-positive long tubes were unexpectedly induced by starvation of the cells, and interestingly, either MTMR6 or Rab1B RNAi significantly inhibited their formation (Fig. 7*A*). These results indicate that MTMR6 and Rab1B are involved in tube formation. Because such peculiar long tubes had not been previously reported, the tubes were further characterized to clarify the significance of our findings.

Intriguingly, when autophagic cells expressing EGFP-DFCP1 were stained with the antibody against the isolation membrane marker Atg16L, several Atg16L-positive granules were found in

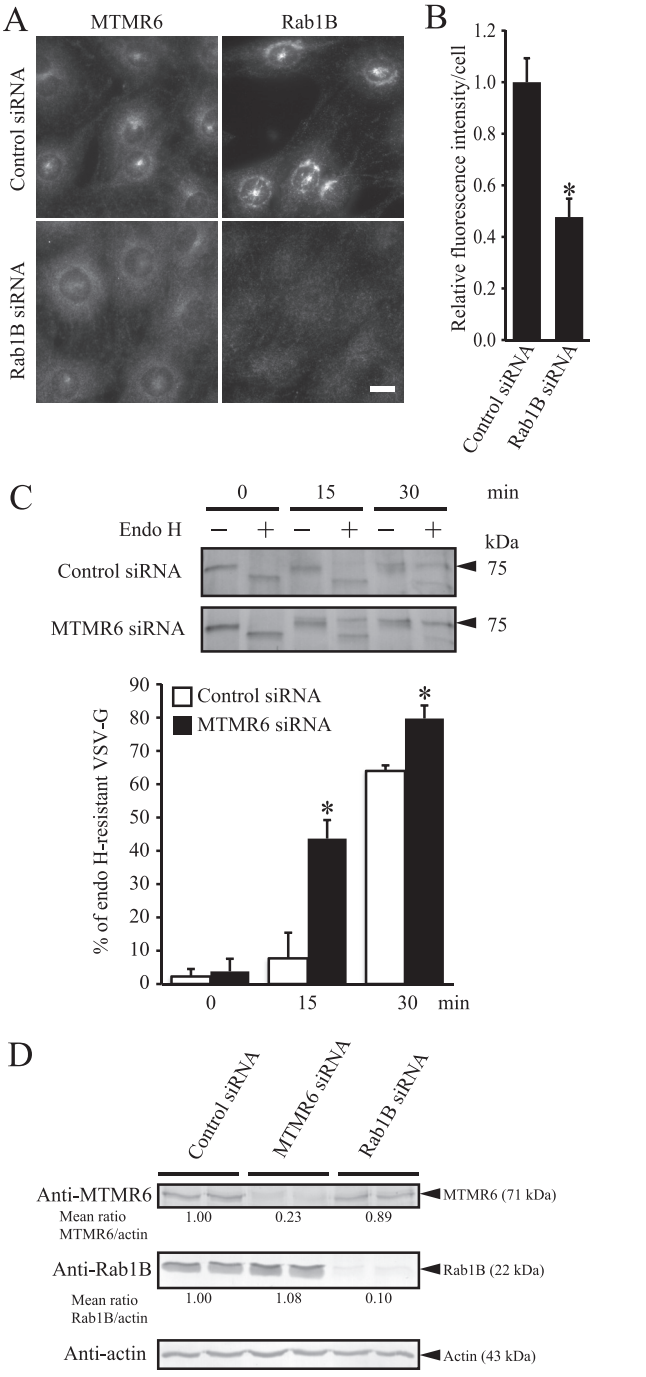

FIGURE 6. **The localization of MTMR6 is regulated by Rab1B, and MTMR6 is related to the secretory pathway.** *A*, the effect of Rab1B knockdown on the localization of MTMR6. Rab1B was knocked down by RNAi in NRK cells and stained with an anti-MTMR6 or anti-Rab1B antibody. *B*, the fluorescence intensity of accumulated MTMR6 staining was quantified by image analysis. The *asterisk* indicates a significant difference from the control (mean ± S.E. (*error bars*); control siRNA, $n = 114$; Rab1B siRNA, $n = 68$; *, $p < 0.001$). *C*, sensitivity of VSV-G to digestion by endo H. NRK cells stably expressing Myc-tagged VSV-G were treated with control or MTMR6 siRNA for 2 days. The cells were then incubated for 12 h at 40 °C. The cells were collected at each time point after the temperature was changed to 32 °C. The VSV-G was immunoprecipitated, treated with or without endo H, and detected with an anti-Myc antibody by Western blotting. *Graph*, the bands of the VSV-G protein were quantified by densitometry, and the ratios of the endo H-resistant VSV-G protein were calculated. A two-way analysis of variance was performed. The *asterisks* indicate a significant difference from the control at each time point (mean ± S.E. (*error bars*); $n = 3$; *, $p < 0.05$). *D*, the effect of MTMR6 or Rab1B RNAi on the amount of MTMR6 and Rab1B was analyzed by Western blotting. The bands were quantified in duplicate, and 100 μg of protein was loaded in each lane. The bands were quantified by densitometry, and actin was used as a loading control. *Bar*, 10 μm.

the tubes (Fig. 7*B*). The granules were also positive for LC3 (Fig. 7*C*). Additionally, some tubes were also faintly positive for LC3, whereas in others, it was hard to observe the signal (Fig. 7*C*). The tubes did not contain the ER marker enzyme protein-disulfide isomerase, indicating that they are distinct from ER (Fig. 7*D*). Furthermore, as shown in Fig. 7*E*, the tubes were LysoTracker-negative and void of an acidic compartment. From these results, we hypothesized that the omegasome function is disrupted by the overexpression of DFCP1 and that elongated tubular omegasomes containing multiple immature autophagosomes are generated.

When the autophagic cells expressing EGFP-DFCP1 were analyzed by transmission electron microscopy, membrane structures containing multiple autophagosome-like granules were observed in the cell (Fig. 7*F*). Furthermore, autophagosome-like granules that were surrounded by the elongated membrane were also observed (Fig. 7*F*). Such structures were not observed in autophagic NRK cells not expressing EGFP-DFCP1. These results are consistent with the immunofluorescence analysis and support our hypothesis.

The Dynamics of the Long Tubular Omegasomes—The long tubular omegasomes were further analyzed with time lapse confocal microscopy. This revealed that the tubes were highly mobile and elastic and elongated in an apparently random fashion (Fig. 7*G*, *arrows* and *insets*, and supplemental Video 1). Furthermore, the tubes were unstable and degraded within a certain brief period (Fig. 7*G*, *arrowhead*, and supplemental Video 1). Of note, the fusion of vesicular omegasomes was not observed. Similar tubes were also observed in a stable NIH3T3 cell line expressing EGFP-DFCP1, indicating that such tube formation is not exclusive to NRK cells (supplemental Video 2). These results suggest that the long tubular omegasomes were unstable structures in cells and that they were formed by the aberrant elongation of the omegasome in EGFP-DFCP1-expressing cells.

The Mechanism of Tubular Omegasome Formation—To address the mechanism of tubular omegasome formation, two DFCP1 mutants were expressed in NRK cells (Fig. 8*A*). The ER-targeting and FYVE domains are reported to be essential for the localization of DFCP1 to the omegasomes (48). DFCP1 Δ-N, which contained only these two domains, was sufficient to form the tubular omegasomes (Fig. 8*A*). In contrast, the double FYVE domain mutant DFCP1 did not exhibit long tubular omegasome formation (Fig. 8*A*). Therefore, the PI(3)P binding activity of DFCP1 is essential for tube formation. When the amount of DFCP1 mRNA was determined using real time PCR, ~80 times more DFCP1 mRNA was detected in our stable cell line than in NRK cells (Fig. 8*B*). Moreover, EGFP-DFCP1 protein was detected by Western blotting in our stable cell line with anti-DFCP1 antibody that recognizes mouse and rat DFCP1 (Fig. 8*C* and supplemental Fig. S1C). However, endogenous DFCP1 protein was undetectable in NRK cells (Fig. 8*C*). When the amount of cell lysate was reduced to 25 μg, the signal of EGFP-DFCP1 was very faint but still detectable (Fig. 8*C*). These

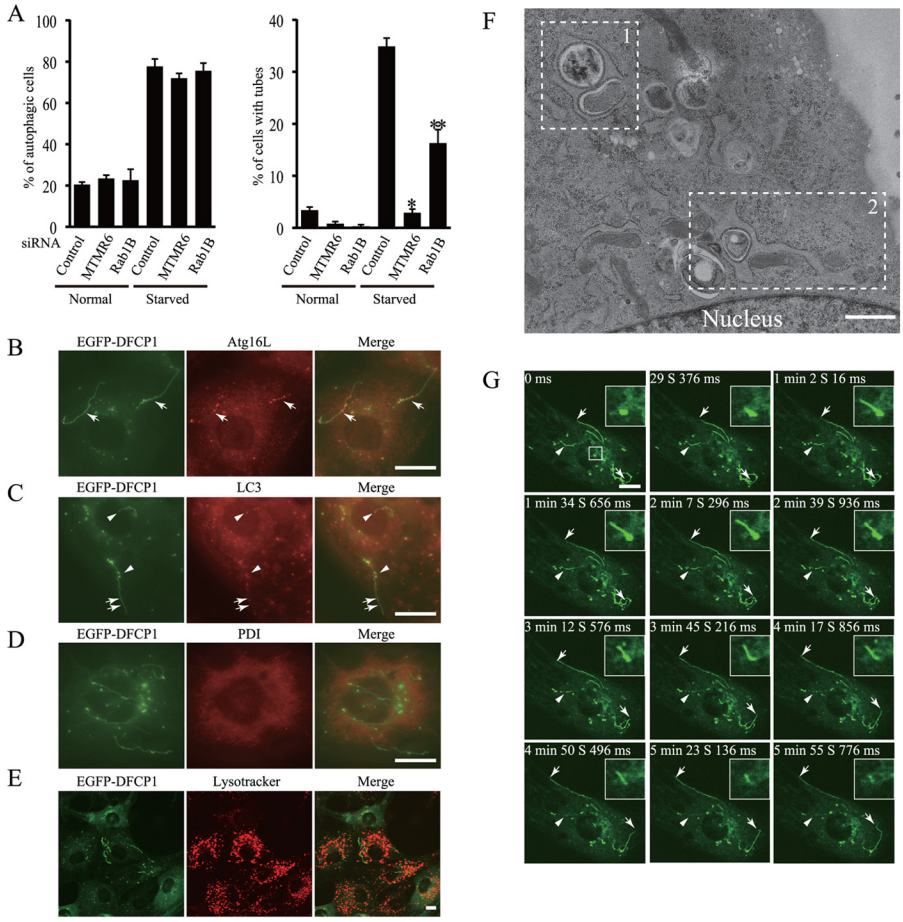

FIGURE 7. **MTMR6 and Rab1B are related to the regulation of the omegasome.** *A*, a stable NRK cell line expressing EGFP-DFCP1 was starved for 60 min, and the number of the autophagic cells that contained more than 10 DFCP1-positive vesicles was counted (*left panel*). The cells that contained the long tubes were excluded from this counting. The cells that contained DFCP1-positive tubes were also counted in the same specimens (*right panel*). Each *bar* indicates the mean ratio of the cells from three independent cover glasses. On each cover glass, more than 100 cells were counted. The asterisks indicate a significant difference from control (mean ± S.E. (*error bars*); $n = 3$; *, $p < 0.001$; **, $p < 0.01$). *B–D*, immunostaining of the stable cell line under the autophagic condition. The cells were starved for 120 min and stained with an anti-Atg16L (*B*), -LC3 (*C*), or -protein-disulfide isomerase (*PDI*) (*D*) antibody, respectively. *Arrows* indicate the tubes that contain Atg16L-positive granules (*B*). *Arrowheads* indicate the tubes that contain LC3-positive granules. A part of the lower tube is faintly positive to LC3 (*paired arrows*) (*C*). *E*, a stable NRK cell line expressing EGFP-DFCP1 was starved for 60 min in Earle's balanced salt solution supplemented with a LysoTracker probe. *F*, transmission electron microscopy of the tubular omegasomes. Two autophagosome-like granules are included in one membrane structure (*dashed box 1*). The autophagosome-like granule is surrounded by the elongated membrane structure (*dashed box 2*). *G*, a stable NRK cell line expressing EGFP-DFCP1 was starved for 60 min, and DFCP1-positive tubes were analyzed by time lapse confocal microscopy. *Arrows* indicate the tips of the elongating tubes. The *arrowhead* indicates a degrading tube. The *insets* show an enlarged view of the magnified *boxed* regions. This granule repeated the elongation and retraction and then faded. The frames corresponding to the tubes are depicted in supplemental Video 1. Bars, 10 μm in *B–E* and *G* and 1 μm in *F*.

data indicate that expression of DFCP1 protein is at least 10-fold higher in our stable cell line than in original NRK cells.

Taken together, these results suggest that the binding of excess EGFP-DFCP1 to PI(3)P induces the formation of abnormally long tubular omegasomes. Namely, a decrease in functional PI(3)P in the omegasome causes tube formation. MTMR6 or Rab1B RNAi significantly inhibited tube formation, indicating that MTMR6 and Rab1B regulate the amount of PI(3)P in the omegasome.

DISCUSSION

Here we have analyzed the cellular localization of endogenous MTMR6 and shown that MTMR6 is present in the cytoplasm and in a condensed form in the pcIC and the peri-Golgi regions (Figs. 1 and 4). Searching for the proteins that regulate the localization of MTMR6, Rab1B was identified as a low affinity or transiently interacting protein that interacts with MTMR6 via the GRAM domain (Fig. 3). The GRAM domain is thought to interact with PI(3)P, PI(5)P, and PI(3,5)P_2 and to regulate the enzyme activity and cellular localization of several MTM phosphatases (32, 39, 40, 41, 51, 52). On the issue of interaction with MTMR6, two groups examined the lipid binding activity of the GRAM domain. However, the specificity of the binding was not consistent, and its lipid binding activity thus remains elusive (32, 52). In our study, the cellular localization of MTMR6 was disrupted by Rab1B RNAi but not wortmannin, indicating that the MTMR6 GRAM domain is a protein-protein-interacting module that regulates the cellular localization of MTMR6 (Figs. 1*E* and 6*A*). Rab1B associates with the membrane by means of the GDP/GTP cycle, and its guanine nucleotide exchange factor is localized on the Golgi membrane (53). MTMR6 preferentially associated with GDP-bound Rab1B (Fig. 3*B*), and expression of EGFP-Rab1B S25N significantly reduced the accumulation of MTMR6 (Fig. 5*B*). MTMR6 was not found on the membrane in cells (Figs. 1*D*,

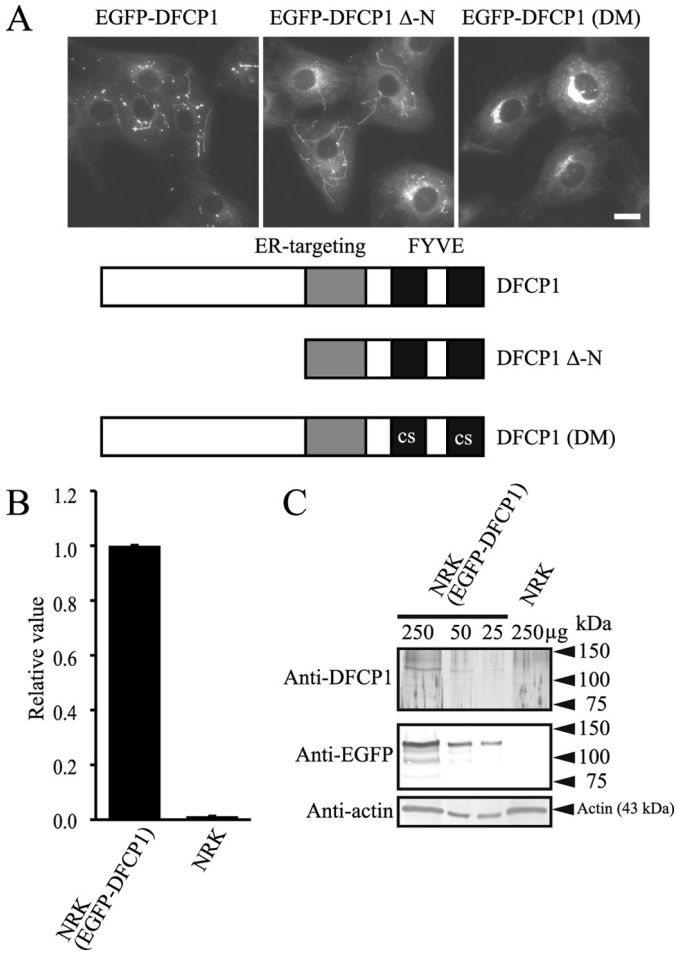

FIGURE 8. **The mechanism of tubular omegasome formation.** *A*, domain of DFCP1 responsible for tubular omegasome formation. Stable NRK cell lines expressing EGFP-DFCP1, EGFP-DFCP1 Δ-N, and EGFP-DFCP1 (domain mutant (*DM*)) were starved for 120 min and observed with fluorescence microscopy. The diagrams show the structure of the constructs. *CS*, mutated FYVE domain. *B*, comparison of the amount of DFCP1 mRNA. The amount of DFCP1 mRNA was quantified by real time PCR. As our stable cell line expresses both EGFP-tagged recombinant mouse and endogenous rat DFCP1, PCR primers were designed to amplify both cDNA fragments (mean ± S.E. (*error bars*); $n = 4$). *C*, comparison of the amount of DFCP1 protein. Cell lysates were analyzed with anti-DFCP1 and EGFP antibodies by Western blotting. The *numbers* at the *top* indicate the amount of protein loaded, and the *numbers* on the *right* are molecular mass markers. Actin was used as a loading control. *Bar,* 10 μm.

inset, and 4*A*, *inset*). We propose that MTMR6 is recruited to the membrane with GDP-bound Rab1B, dephosphorylates substrates there, and ultimately is released into the cytosol after the GDP/GTP exchange of Rab1B.

We further found that other GRAM domain-containing MTM phosphatases also interact with GDP-bound Rab1B (Fig. 3*D*). MTMR6 and MTMR7, which have a close phylogenetic relationship, preferentially bound to Rab1B S22N (Fig. 3*D*). We have previously reported that MTMR7 is condensed at the perinuclear region in N1E-115 neuroblastoma cells (6). Therefore, Rab1B might recruit MTMR7 to that same region in neuronal cells. In addition, although the affinity of the other MTM phosphatases to Rab1B S22N was lower than that of MTMR6 and MTMR7, it is possible that they interact with other Rabs and are concentrated to certain specific regions in cells. The substrate specificity of MTM phosphatases is considered to be highly similar, and the disruption of each enzyme results in a different phenotype (1, 3, 4, 11–14). Therefore, we think it is highly likely that specific Rab proteins transiently bind to the GRAM domain and regulate the localization of each MTM phosphatase in cells.

MTMR6 was condensed in the pcIC and the peri-Golgi regions and overlapped with certain endosomal and Golgi markers (Figs. 1, *C*, *D*, and *F*, and 4, *A* and *B*). The early endosomes move along the microtubule toward the microtubule-organizing center, and in most cells (*e.g.* late endosomes, recycling endosomes, and lysosomes), they are observed in close proximity to the nucleus (54–56). In the case of autophagy, autophagosomes are formed at the cell periphery, move along the microtubule toward the microtubule-organizing center, and are fused with lysosomes in the perinuclear region (57). Therefore, many kinds of transport vesicles seem to be able to utilize the activity of MTMR6 to dephosphorylate the 3-phosphoinositide lipids on their membrane. We identified Rab1B as a regulator of the localization of MTMR6 and demonstrated that it concentrated MTMR6 to the pcIC and the peri-Golgi regions (Fig. 6, *A* and *B*). MTMR6 is particularly highly concentrated in the pcIC, which is also referred as the "endoplasmic reticulum-Golgi intermediate compartment." The interaction of MTMR6 with Rab1B in these regions strongly suggests that MTMR6 is related to the secretory pathway because Rab1B is known to play a key role in ER-Golgi and intra-Golgi transport (45). Although PI(3)P and PI(3,5)P_2 have not been reportedly detected on the pcIC and Golgi membranes, PI3K-C2α and VPS34 have been observed in the Golgi area (58, 59). The localization of PI 3-kinases and PI 3-phosphatase suggests the existence of 3-phosphoinositide lipid metabolism in the vicinity of the Golgi. The reduction in the level of MTMR6 accelerated the transport of VSV-G, indicating that MTMR6 is related to the secretory pathway and negatively regulates protein transport. Our results do not rule out a relationship of MTMR6 with other transport pathways, and further analysis is essential to clarify in detail the 3-phosphoinositide lipid metabolism in the Golgi area.

We found that MTMR6 and Rab1B RNAi significantly inhibits the aberrant elongation of the omegasome membrane; this is caused by a decrease in functional PI(3)P in the omegasome. We assume that MTMR6 and Rab1B RNAi increases the local PI(3)P level on the omegasome membrane and might restore the binding of regulatory proteins, thereby inhibiting aberrant tubular omegasome formation. Consequently, we propose that Rab1B concentrates MTMR6 on the omegasome and regulates the PI(3)P level and that these functions are both related to the proper regulation of the omegasome membrane.

In addition to MTMR6, MTMR3 and MTMR14 are also reported to be involved in autophagy, and their knockdown resulted in autophagosome formation even in a nutrient-rich condition (33, 49). For MTMR6, we did not observe the induction of autophagy after a reduction in MTMR6 in normal growth medium (Fig. 7*A*). We showed that the binding of MTMR3 to Rab1B was undetectable by immunoprecipitation (Fig. 3*D*) and that MTMR14 lacks the GRAM domain (33). This evidence suggests that the function of MTMR6 is different from that of the other MTM phosphatases and that MTMR6 dephosphorylates the specific pool of PI(3)P in the case of autophagy.

Very recently, Zou *et al.* (60) reported that the MTMR8-MTMR9 complex is also involved in autophagosome formation. Because rodents do not possess the MTMR8 gene, MTMR6 may compensate for some functions of MTMR8 in rodents.

Acknowledgment—We thank Dr. Kevin Boru of Pacific Edit for review of the manuscript.

REFERENCES

1. Laporte, J., Hu, L. J., Kretz, C., Mandel, J. L., Kioschis, P., Coy, J. F., Klauck, S. M., Poustka, A., and Dahl, N. (1996) A gene mutated in X-linked myotubular myopathy defines a new putative tyrosine phosphatase family conserved in yeast. *Nat. Genet.* **13,** 175–182
2. Alonso, A., Sasin, J., Bottini, N., Friedberg, I., Friedberg, I., Osterman, A., Godzik, A., Hunter, T., Dixon, J., and Mustelin, T. (2004) Protein tyrosine phosphatases in the human genome. *Cell* **117,** 699–711
3. Robinson, F. L., and Dixon, J. E. (2006) Myotubularin phosphatases: policing 3-phosphoinositides. *Trends Cell Biol.* **16,** 403–412
4. Tosch, V., Rohde, H. M., Tronchère, H., Zanoteli, E., Monroy, N., Kretz, C., Dondaine, N., Payrastre, B., Mandel, J. L., and Laporte, J. (2006) A novel PI3P and PI(3,5)P2 phosphatase with an inactivating variant in centronuclear myopathy. *Hum. Mol. Genet.* **15,** 3098–3106
5. Kim, S. A., Vacratsis, P. O., Firestein, R., Cleary, M. L., and Dixon, J. E. (2003) Regulation of myotubularin-related (MTMR)2 phosphatidylinositol phosphatase by MTMR5, a catalytically inactive phosphatase. *Proc. Natl. Acad. Sci. U.S.A.* **100,** 4492–4497
6. Mochizuki, Y., and Majerus, P. W. (2003) Characterization of myotubularin-related protein 7 and its binding partner, myotubularin-related protein 9. *Proc. Natl. Acad. Sci. U.S.A.* **100,** 9768–9773
7. Nandurkar, H. H., Layton, M., Laporte, J., Selan, C., Corcoran, L., Caldwell, K. K., Mochizuki, Y., Majerus, P. W., and Mitchell, C. A. (2003) Identification of myotubularin as the lipid phosphatase catalytic subunit associated with the 3-phosphatase adapter protein, 3-PAP. *Proc. Natl. Acad. Sci. U.S.A.* **100,** 8660–8665
8. Robinson, F. L., and Dixon, J. E. (2005) The phosphoinositide-3-phosphatase MTMR2 associates with MTMR13, a membrane-associated pseudophosphatase also mutated in type 4B Charcot-Marie-Tooth disease. *J. Biol. Chem.* **280,** 31699–31707
9. Berger, P., Berger, I., Schaffitzel, C., Tersar, K., Volkmer, B., and Suter, U. (2006) Multi-level regulation of myotubularin-related protein-2 phosphatase activity by myotubularin-related protein-13/set-binding factor-2. *Hum. Mol. Genet.* **15,** 569–579
10. MacKay, C., Déclais, A. C., Lundin, C., Agostinho, A., Deans, A. J., MacArtney, T. J., Hofmann, K., Gartner, A., West, S. C., Helleday, T., Lilley, D. M., and Rouse, J. (2010) Identification of KIAA1018/FAN1, a DNA repair nuclease recruited to DNA damage by monoubiquitinated FANCD2. *Cell* **142,** 65–76
11. Bolino, A., Muglia, M., Conforti, F. L., LeGuern, E., Salih, M. A., Georgiou, D. M., Christodoulou, K., Hausmanowa-Petrusewicz, I., Mandich, P., Schenone, A., Gambardella, A., Bono, F., Quattrone, A., Devoto, M., and Monaco, A. P. (2000) Charcot-Marie-Tooth type 4B is caused by mutations in the gene encoding myotubularin-related protein-2. *Nat. Genet.* **25,** 17–19
12. Azzedine, H., Bolino, A., Taïeb, T., Birouk, N., Di Duca, M., Bouhouche, A., Benamou, S., Mrabet, A., Hammadouche, T., Chkili, T., Gouider, R., Ravazzolo, R., Brice, A., Laporte, J., and LeGuern, E. (2003) Mutations in MTMR13, a new pseudophosphatase homologue of MTMR2 and Sbf1, in two families with an autosomal recessive demyelinating form of Charcot-Marie-Tooth disease associated with early-onset glaucoma. *Am. J. Hum. Genet.* **72,** 1141–1153
13. Senderek, J., Bergmann, C., Weber, S., Ketelsen, U. P., Schorle, H., Rudnik-Schöneborn, S., Büttner, R., Buchheim, E., and Zerres, K. (2003) Mutation of the SBF2 gene, encoding a novel member of the myotubularin family, in Charcot-Marie-Tooth neuropathy type 4B2/11p15. *Hum. Mol. Genet.* **12,** 349–356
14. Firestein, R., Nagy, P. L., Daly, M., Huie, P., Conti, M., and Cleary, M. L. (2002) Male infertility, impaired spermatogenesis, and azoospermia in mice deficient for the pseudophosphatase Sbf1. *J. Clin. Investig.* **109,** 1165–1172
15. Shen, J., Yu, W. M., Brotto, M., Scherman, J. A., Guo, C., Stoddard, C., Nosek, T. M., Valdivia, H. H., Qu, C. K. (2009) Deficiency of MIP/MTMR14 phosphatase induces a muscle disorder by disrupting Ca^{2+} homeostasis. *Nat. Cell Biol.* **11,** 769–776
16. Yanagiya, T., Tanabe, A., Iida, A., Saito, S., Sekine, A., Takahashi, A., Tsunoda, T., Kamohara, S., Nakata, Y., Kotani, K., Komatsu, R., Itoh, N., Mineo, I., Wada, J., Masuzaki, H., Yoneda, M., Nakajima, A., Miyazaki, S., Tokunaga, K., Kawamoto, M., Funahashi, T., Hamaguchi, K., Tanaka, K., Yamada, K., Hanafusa, T., Oikawa, S., Yoshimatsu, H., Nakao, K., Sakata, T., Matsuzawa, Y., Kamatani, N., Nakamura, Y., and Hotta, K. (2007) Association of single-nucleotide polymorphisms in MTMR9 gene with obesity. *Hum. Mol. Genet.* **16,** 3017–3026
17. Hotta, K., Kitamoto, T., Kitamoto, A., Mizusawa, S., Matsuo, T., Nakata, Y., Kamohara, S., Miyatake, N., Kotani, K., Komatsu, R., Itoh, N., Mineo, I., Wada, J., Yoneda, M., Nakajima, A., Funahashi, T., Miyazaki, S., Tokunaga, K., Masuzaki, H., Ueno, T., Hamaguchi, K., Tanaka, K., Yamada, K., Hanafusa, T., Oikawa, S., Yoshimatsu, H., Sakata, T., Matsuzawa, Y., Nakao, K., and Sekine, A. (2011) Association of variations in the FTO, SCG3 and MTMR9 genes with metabolic syndrome in a Japanese population. *J. Hum. Genet.* **56,** 647–651
18. Taylor, G. S., Maehama, T., and Dixon, J. E. (2000) Myotubularin, a protein tyrosine phosphatase mutated in myotubular myopathy, dephosphorylates the lipid second messenger, phosphatidylinositol 3-phosphate. *Proc. Natl. Acad. Sci. U.S.A.* **97,** 8910–8915
19. Maffucci, T., Brancaccio, A., Piccolo, E., Stein, R. C., and Falasca, M. (2003) Insulin induces phosphatidylinositol-3-phosphate formation through TC10 activation. *EMBO J.* **22,** 4178–4189
20. Maffucci, T., Cooke, F. T., Foster, F. M., Traer, C. J., Fry, M. J., and Falasca, M. (2005) Class II phosphoinositide 3-kinase defines a novel signaling pathway in cell migration. *J. Cell Biol.* **169,** 789–799
21. Funderburk, S. F., Wang, Q. J., and Yue, Z. (2010) The Beclin 1-VPS34 complex—at the crossroads of autophagy and beyond. *Trends Cell Biol.* **20,** 355–362
22. Rudge, S. A., Anderson, D. M., and Emr, S. D. (2004) Vacuole size control: regulation of PI(3,5)P2 levels by the vacuole-associated Vac14-Fig 4 complex, a PI(3,5)P2-specific phosphatase. *Mol. Biol. Cell* **15,** 24–36
23. Ivetac, I., Munday, A. D., Kisseleva, M. V., Zhang, X. M., Luff, S., Tiganis, T., Whisstock, J. C., Rowe, T., Majerus, P. W., and Mitchell, C. A. (2005) The type Iα inositol polyphosphate 4-phosphatase generates and terminates phosphoinositide 3-kinase signals on endosomes and the plasma membrane. *Mol. Biol. Cell* **16,** 2218–2233
24. Kong, A. M., Horan, K. A, Sriratana, A., Bailey, C. G., Collyer, L. J., Nandurkar, H. H., Shisheva, A., Layton, M. J., Rasko, J. E., Rowe, T., and Mitchell, C. A. (2006) Phosphatidylinositol 3-phosphate [PI3P] is generated at the plasma membrane by an inositol polyphosphate 5-phosphatase: endogenous PI3P can promote GLUT4 translocation to the plasma membrane. *Mol. Cell. Biol.* **26,** 6065–6081
25. Clague, M. J., Urbé, S., and de Lartigue, J. (2009) Phosphoinositides and the endocytic pathway. *Exp. Cell Res.* **315,** 1627–1631
26. Michell, R. H., Heath, V. L., Lemmon, M. A., and Dove, S. K. (2006) Phosphatidylinositol 3,5-bisphosphate: metabolism and cellular functions. *Trends Biochem. Sci.* **31,** 52–63
27. Dove, S. K., Cooke, F. T., Douglas, M. R., Sayers, L. G., Parker, P. J., and Michell, R. H. (1997) Osmotic stress activates phosphatidylinositol-3,5-bisphosphate synthesis. *Nature* **390,** 187–192
28. Jones, D. R., González-García, A., Díez, E., Martinez-A, C., Carrera, A. C., and Meŕida, I. (1999) The identification of phosphatidylinositol 3,5-bisphosphate in T-lymphocytes and its regulation by interleukin-2. *J. Biol. Chem.* **274,** 18407–18413
29. de Lartigue, J., Polson, H., Feldman, M., Shokat, K., Tooze, S. A., Urbé, S., and Clague, M. J. (2009) PIKfyve regulation of endosome-linked pathways. *Traffic* **10,** 883–893
30. Ferguson, C. J., Lenk, G. M., and Meisler, M. H. (2009) Defective au-

tophagy in neurons and astrocytes from mice deficient in $PI(3,5)P_2$. *Hum. Mol. Genet.* **18,** 4868–4878
31. Srivastava, S., Li, Z., Lin, L., Liu, G., Ko, K., Coetzee, W. A., and Skolnik, E. Y. (2005) The phosphatidylinositol 3-phosphate phosphatase myotubularin-related protein 6 (MTMR6) is a negative regulator of the Ca^{2+}-activated K^+ channel KCa3.1. *Mol. Cell. Biol.* **25,** 3630–3638
32. Zou, J., Chang, S. C., Marjanovic, J., and Majerus, P. W. (2009) MTMR9 increases MTMR6 enzyme activity, stability, and role in apoptosis. *J. Biol. Chem.* **284,** 2064–2071
33. Vergne, I., Roberts, E., Elmaoued, R. A., Tosch, V., Delgado, M. A., Proikas-Cezanne, T., Laporte, J., and Deretic, V. (2009) Control of autophagy initiation by phosphoinositide 3-phosphatase Jumpy. *EMBO J.* **28,** 2244–2258
34. Dang, H., Li, Z., Skolnik, E. Y., and Fares, H. (2004) Disease-related myotubularins function in endocytic traffic in Caenorhabditis elegans. *Mol. Biol. Cell* **15,** 189–196
35. Silhankova, M., Port, F., Harterink, M., Basler, K., and Korswagen, H. C. (2010) Wnt signalling requires MTM-6 and MTM-9 myotubularin lipid-phosphatase function in Wnt-producing cells. *EMBO J.* **29,** 4094–4105
36. Tanaka, T., Takeno, T., Watanabe, Y., Uchiyama, Y., Murakami, T., Yamashita, H., Suzuki, A., Aoi, R., Iwanari, H., Jiang, S. Y., Naito, M., Tachibana, K., Doi, T., Shulman, A. I., Mangelsdorf, D. J., Reiter, R., Auwerx, J., Hamakubo, T., and Kodama, T. (2002) The generation of monoclonal antibodies against human peroxisome proliferator-activated receptors (PPARs). *J. Atheroscler. Thromb.* **9,** 233–242
37. Saitoh, R., Ohtomo, T., Yamada, Y., Kamada, N., Nezu, J., Kimura, N., Funahashi, S., Furugaki, K., Yoshino, T., Kawase, Y., Kato, A., Ueda, O., Jishage, K., Suzuki, M., Fukuda, R., Arai, M., Iwanari, H., Takahashi, K., Sakihama, T., Ohizumi, I., Kodama, T., Tsuchiya, M., and Hamakubo, T. (2007) Viral envelope protein gp64 transgenic mouse facilitates the generation of monoclonal antibodies against exogenous membrane proteins displayed on baculovirus. *J. Immunol. Methods* **322,** 104–117
38. Daigo, K., Kawamura, T., Ohta, Y., Ohashi, R., Katayose, S., Tanaka, T., Aburatani, H., Naito, M., Kodama, T., Ihara, S., and Hamakubo, T. (2011) Proteomic analysis of native hepatocyte nuclear factor-4α (HNF4α) isoforms, phosphorylation status, and interactive cofactors. *J. Biol. Chem.* **286,** 674–686
39. Berger, P., Schaffitzel, C., Berger, I., Ban, N., and Suter, U. (2003) Membrane association of myotubularin-related protein 2 is mediated by a pleckstrin homology-GRAM domain and a coiled-coil dimerization module. *Proc. Natl. Acad. Sci. U.S.A.* **100,** 12177–12182
40. Tsujita, K., Itoh, T., Ijuin, T., Yamamoto, A., Shisheva, A., Laporte, J., and Takenawa, T. (2004) Myotubularin regulates the function of the late endosome through the gram domain-phosphatidylinositol 3,5-bisphosphate interaction. *J. Biol. Chem.* **279,** 13817–13824
41. Lorenzo, O., Urbé, S., and Clague, M. J. (2005) Analysis of phosphoinositide binding domain properties within the myotubularin-related protein MTMR3. *J. Cell Sci.* **118,** 2005–2012
42. Ullrich, O., Reinsch, S., Urbé, S., Zerial, M., and Parton, R. G. (1996) Rab11 regulates recycling through the pericentriolar recycling endosome. *J. Cell Biol.* **135,** 913–924
43. Marie, M., Dale, H. A., Sannerud, R., and Saraste, J. (2009) The function of the intermediate compartment in pre-Golgi trafficking involves its stable connection with the centrosome. *Mol. Biol. Cell* **20,** 4458–4470
44. Alvarez, C., Garcia-Mata, R., Brandon, E., and Sztul, E. (2003) COPI recruitment is modulated by a Rab1b-dependent mechanism. *Mol. Biol. Cell* **14,** 2116–2127
45. Hutagalung, A. H., and Novick, P. J. (2011) Role of Rab GTPases in membrane traffic and cell physiology. *Physiol. Rev.* **91,** 119–149
46. Zoppino, F. C., Militello, R. D., Slavin, I., Alvarez, C., and Colombo, M. I. (2010) Autophagosome formation depends on the small GTPase Rab1 and functional ER exit sites. *Traffic* **11,** 1246–1261
47. Huang, J., Birmingham, C. L., Shahnazari, S., Shiu, J., Zheng, Y. T., Smith, A. C., Campellone, K. G., Heo, W. D., Gruenheid, S., Meyer, T., Welch, M. D., Ktistakis, N. T., Kim, P. K., Klionsky, D. J., and Brumell, J. H. (2011) Antibacterial autophagy occurs at PI(3)P-enriched domains of the endoplasmic reticulum and requires Rab1 GTPase. *Autophagy* **7,** 17–26
48. Axe, E. L., Walker, S. A., Manifava, M., Chandra, P., Roderick, H. L., Habermann, A., Griffiths, G., and Ktistakis, N. T. (2008) Autophagosome formation from membrane compartments enriched in phosphatidylinositol 3-phosphate and dynamically connected to the endoplasmic reticulum. *J. Cell Biol.* **182,** 685–701
49. Taguchi-Atarashi, N., Hamasaki, M., Matsunaga, K., Omori, H., Ktistakis, N. T., Yoshimori, T., and Noda, T. (2010) Modulation of local PI3P levels by the PI phosphatase MTMR3 regulates constitutive autophagy. *Traffic* **11,** 468–478
50. Winslow, A. R., Chen, C. W., Corrochano, S., Acevedo-Arozena, A., Gordon, D. E., Peden, A. A., Lichtenberg, M., Menzies, F. M., Ravikumar, B., Imarisio, S., Brown, S., O'Kane, C. J., and Rubinsztein, D. C. (2010) α-Synuclein impairs macroautophagy: implications for Parkinson's disease. *J. Cell Biol.* **190,** 1023–1037
51. Schaletzky, J., Dove, S. K., Short, B., Lorenzo, O., Clague, M. J., and Barr, F. A. (2003) Phosphatidylinositol-5-phosphate activation and conserved substrate specificity of the myotubularin phosphatidylinositol 3-phosphatases. *Curr. Biol.* **13,** 504–509
52. Choudhury, P., Srivastava, S., Li, Z., Ko, K., Albaqumi, M., Narayan, K., Coetzee, W. A., Lemmon, M. A., and Skolnik, E. Y. (2006) Specificity of the myotubularin family of phosphatidylinositol-3-phosphatase is determined by the PH/GRAM domain. *J. Biol. Chem.* **281,** 31762–31769
53. Barrowman, J., Bhandari, D., Reinisch, K., and Ferro-Novick, S. (2010) TRAPP complexes in membrane traffic: convergence through a common Rab. *Nat. Rev. Mol. Cell Biol.* **11,** 759–763
54. Baravalle, G., Schober, D., Huber, M., Bayer, N., Murphy, R. F., and Fuchs, R. (2005) Transferrin recycling and dextran transport to lysosomes is differentially affected by bafilomycin, nocodazole, and low temperature. *Cell Tissue Res.* **320,** 99–113
55. Luzio, J. P., Pryor, P. R., and Bright, N. A. (2007) Lysosomes: fusion and function. *Nat. Rev. Mol. Cell Biol.* **8,** 622–632
56. Seaman, M. N. (2008) Endosome protein sorting: motifs and machinery. *Cell. Mol. Life Sci.* **65,** 2842–2858
57. Yoshimori, T., and Noda, T. (2008) Toward unraveling membrane biogenesis in mammalian autophagy. *Curr. Opin. Cell Biol.* **20,** 401–407
58. Domin, J., Gaidarov, I., Smith, M. E., Keen, J. H., and Waterfield, M. D. (2000) The class II phosphoinositide 3-kinase PI3K-C2α is concentrated in the trans-Golgi network and present in clathrin-coated vesicles. *J. Biol. Chem.* **275,** 11943–11950
59. Kihara, A., Kabeya, Y., Ohsumi, Y., and Yoshimori, T. (2001) Beclin-phosphatidylinositol 3-kinase complex functions at the trans-Golgi network. *EMBO Rep.* **2,** 330–335
60. Zou, J., Zhang, C., Marjanovic, J., Kisseleva, M. V., Majerus, P. W., and Wilson, M. P. (2012) Myotubularin-related protein (MTMR) 9 determines the enzymatic activity, substrate specificity, and role in autophagy of MTMR8. *Proc. Natl. Acad. Sci. U.S.A.* **109,** 9539–9544